Morphological and chemical characterization of microfabricated fibres for biological applications

J. GOLD, B. KASEMO
Department of Applied Physics, Chalmers University of Technology and Göteborg University, S-412 96 Göteborg, Sweden

Monodisperse fibres and particulates of different materials with controllable three-dimensional shape, size and chemical composition are of interest in research on toxic respirable fibres as well as wear debris around orthopaedic implants. We have previously demonstrated the production of well-controlled, metal and oxide microfabricated fibres having dimensions 0.1 to 10 μm. While our previous results focused on how controlled fibres can be *prepared* by microfabrication methods, this paper evaluates *property–production relationships* for microfabricated fibres. Here we have briefly reviewed the production of 0.1 μm × 0.5 μm × 10 μm microfabricated fibres made by electron beam lithography from evaporated titanium or silicon oxide films using a double lift-off method. We have also analysed the properties of these fibres with respect to morphology and chemical composition, and how they are affected by variations in the production process. Two different solution types have been used to place fibres into liquid suspension and to clean and sterilize them for biological testing. One method involves the use of organic solvents; the other a hydroxide solution and water. While fibre dimensions appear to be material-specific, differences can be corrected for by compensation of the size of the lithographic pattern. Similarly the crystallinity of fibres is material-specific, as is to be expected of evaporated thin films, but should be possible to modify by varying deposition parameters or heat treating, for example. Of the cleaning methods used, the one using an aqueous hydroxide solution is preferred over solvent cleaning, as it is easier to perform and appears to be more effective at removing resist from the fibre suspension.

1. Introduction

Metal, oxide, and polymer particulates of $\leqslant 10\,\mu m$ dimensions are important in many human–environment interactions. Examples include inhaled asbestos fibres, which form lung disease and even lung cancer [1], and wear debris-associated bone loss around orthopaedic implants [2, 3]. The mechanisms by which particulates can damage biological tissues are still largely unknown and are currently subject to extensive research. It is generally agreed that both chemical properties and particulate morphology, such as three-dimensional shape (e.g. fibrous versus spherical) and dimensions, play a role in determining cellular responses *in vitro* and *in vivo* [4]. Of major importance, in addition to shape/size, is also the role of surface properties (surface chemistry, roughness, etc.), as the surface forms one side of the particulate–tissue interface [5–7]. Such properties are important for all foreign materials in the body, as surface properties are believed to also play a key role in determining the biocompatibility and success of many medical implants [8, 9].

In order to elucidate possible mechanisms operating during particulate–tissue interactions, the properties of a given particulate test sample is typically varied intentionally in some way, for example, by crushing or grinding to various extents in order to change the size distribution, or by coating the particulates with surfactants or other substances which modify surface chemical properties. In such treatments there is a risk that one accidentally modifies also other properties of the particulate in addition to the one intended by the treatment, with a concomitant risk of drawing the wrong conclusions from the biological results. This risk is even larger when commercially purchased batches of different materials are used. Investigations that are aimed at studying the role of one particulate property frequently use test samples that vary with regard to other properties as well, despite efforts to eliminate such cross-interference.

Researchers studying the mechanisms of particulate-induced tissue diseases have therefore expressed a need for controlled, mono-dispersed test samples which would make it possible to separate shape and dimensional aspects from the chemical properties of micrometre-sized particulates [10, 11]. Specifically one wants to systematically vary one property at time (such as particle or fibre size, shape, or surface chemistry). We have previously described

0957–4530

a method to produce such well-controlled particulates using state-of-the-art microfabrication techniques — originally developed to produce integrated circuits for the microelectronics industry [12] — and have focused on the use of electron beam lithography to produce metal and oxide fibres having dimensions 0.1–10 μm. [13]

Microfabrication techniques offer unprecedented flexibility in the choice of particulate material, shape, and dimensions that can be made. In principle, most materials which can be deposited in thin films, and in a controlled way, can be used to make microfabricated particulates. Particulate shapes and dimensions can be systematically varied by changing their specification in a computer-aided design (CAD) drawing. Monodispersed size distributions are achieved by drawing the same particle pattern millions of times with, for example, a focused electron beam in the case of electron beam lithography. Since electron beam lithography has spatial resolutions down to the order of ten nanometres, it is well suited to make particulates in the size ranges which are relevant to studying the interactions between particulates, biological cells and biological macromolecules, respectively. Although traditionally used to make microelectronics devices, such as transistors, which remain attached to the microchip surface, we have developed the basic microfabrication technique a step further to make possible the removal of microfabricated structures from their substrates, and to suspend them in liquid solutions, for example, water or cell culture media, for biological testing [13].

The focus of this paper is to characterize the morphology and chemical composition of such microfabricated fibres as a complement to the earlier manufacturing-oriented paper [13]. Specific attention has been focused on fibres of dimensions 0.1 μm × 0.5 μm × 10 μm that were produced in titanium or silicon oxide. Fibres of these dimensions are readily inhaled into the lungs [14, 15] and fall within the dimensional range shown to be most carcinogenic in laboratory animals [10]. These particulate materials are also relevant to current issues in the fields of both biomaterials [3, 6] and inhalation toxicology [17], and are known to invoke different biological responses *in vivo* and *in vitro*.

In this paper we further compare the ability of organic versus aqueous solvents to remove and clean fibres, as well as the fibre morphology and surface chemical compositions resulting from these cleaning methods.

2. Materials and methods

2.1. Production of fibres

The production of microfabricated fibres has previously been described in detail by Gold *et al.* [13]. In the present work, fibres having a rectangular cross-section of 0.1 μm × 0.5 μm and a length of 10 μm were made by the double lift-off technique from two materials; titanium and silicon oxide. The process is schematically illustrated in Fig. 1. A silicon wafer is first coated with a layer of polymer resist (polyimide, SAL

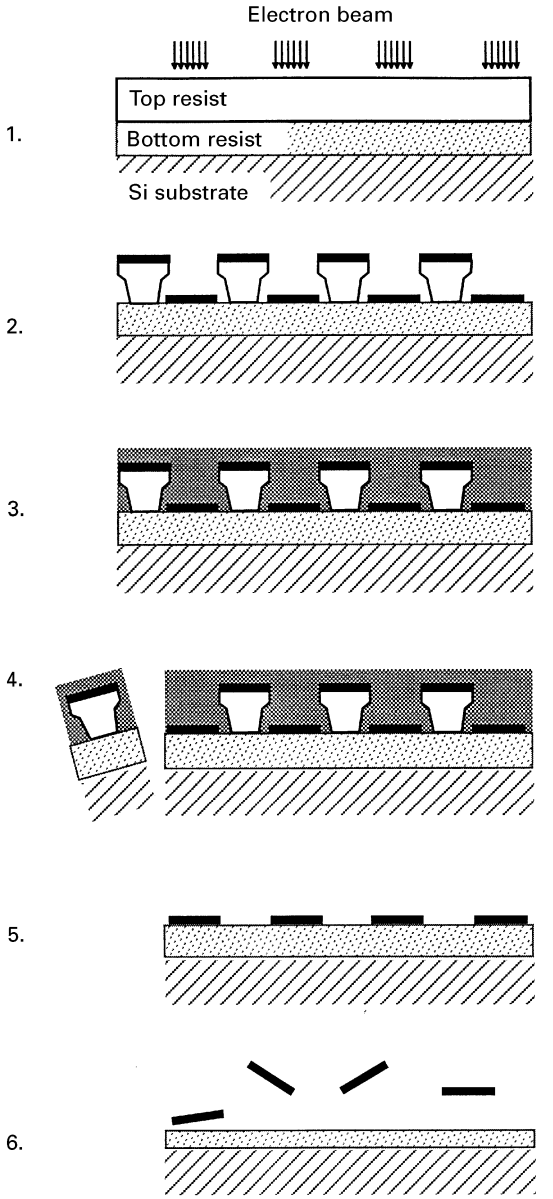

Figure 1 Schematic illustration of the double lift-off technique. Processing steps 1–6 are described in the text.

110, Shipley), followed by a second layer of a positive electron beam resist (ZEP520, Nippon Zeon, Co., Ltd.). A focused electron beam (JEOL JBX 5D-II electron beam lithography system) is used to draw the two-dimensional, rectangular fibre pattern (0.5 μm × 10 μm) ten million times within two 8 mm × 30 mm areas in the top resist layer (step 1). Resist which was exposed by the electron beam is developed away, and a titanium or silicon oxide film (0.1 μm thick) is then deposited onto the patterned resist layers (step 2). The films are deposited by electron beam evaporation of titanium (0.2 nm/s, $0.1–1 \times 10^{-4}$ Pa) or silicon dioxide (99.99% quartz, Balzers, 0.15–0.25 nm/s, $1–2 \times 10^{-4}$ Pa). The entire wafer is then coated with a thin layer of resist (step 3) in order to protect it from damage during the subsequent sawing operation. The two 8 mm × 30 mm sections which contain the fibres are cut from the wafer using a high-speed diamond blade saw (step 4) and are rinsed under a forced water jet to remove silicon dust created during cutting of the wafer. The

remaining top resist and overlying evaporated film + protective resist coating are then completely removed by lift-off in a solvent selectively dissolving the top resist (ethylmethyl-ketone). After this treatment the fibres remain on the bottom resist layer (step 5). Slight dissolution of the bottom resist is then used to release the fibres into liquid suspension (step 6).

Two different solutions were used to remove the fibres from the bottom resist layer, namely an organic solvent (acetone) or an aqueous hydroxide solution. The subsequent fibre cleaning procedure differed depending upon which solution type was used. The two methods are executed as follows:

Cleaning method I

Fibres were removed from the bottom resist layer by ultrasonication in filtered acetone (pro analysis (p.a.) grade) for 2 min, followed by centrifugation at 5500 r.p.m. for 10 min and a quick dip in the ultrasonic bath to loosen the fibres from the bottom of the centrifuge tube. The fibre suspension was then filtered in a suction filter apparatus using 0.2 μm or 0.4 μm pore size Isopore™ track-etched membrane filters (polycarbonate, Millipore). Fibres were soaked and rinsed three times in each of pre-filtered analysis grade (p.a.) acetone, methyl alcohol and ethyl alcohol, by turning off the suction to the filter apparatus and adding the rinsing liquid. Sterilization, performed prior to biological experiments and characterization analysis, was achieved by similarly soaking fibres on the filter in 70% ethyl alcohol/sterile water solution (sterile water = autoclaved, endotoxin-free), followed by copious rinsing with sterile water, and drying by filtering air-only through the filter apparatus.

The filter membrane with adherent fibres was carefully removed from the filter apparatus and placed in a sterile centrifuge tube. The tube was filled with sterile water and was centrifuged at 5500 r.p.m. for 10 min until the fibres were removed from the filter. A pipette was used to withdraw fibre samples from the bottom of the centrifuge tube and to place droplets of fibre suspension on the appropriate substrates for analysis. Droplets were allowed to dry in air or on a hot plate at 90 °C. Processing was performed in Class 10,000 or Class 100 clean rooms.

Cleaning method II

Fibres were removed from the bottom resist layer by first immersing the fibre-containing chip in a filtered developer solution for SAL110 (SAL101 : tetraethyl ammonium hydroxide solution, Shipley Corp.) diluted 1 : 1 in purified water (18.2 MΩcm Milli-Q water, Millipore) for 1 min, followed by ultra-sonication for 2 min, and centrifugation at 5500 r.p.m. for 10 min. The centrifuge tube was then quickly dipped in an ultrasonic bath to loosen the fibres from the bottom, and the fibre suspension was poured onto a 0.5 μm pore sized Fluoropore® filter (unlaminated PTFE membrane, Millipore) in a suction filter apparatus. Fibres were soaked for about 1 min and rinsed three times in filtered diluted SAL101. This procedure was then repeated with sterile water. Fibres were sterilized, dried, and handled as described above for cleaning method I. The hydrophobic Teflon™ filter membrane was first rinsed with methanol prior to filtering aqueous solutions.

2.2 Fibre characterization

Electron microscopy

Fibres were examined using a JEOL JSM 6301F scanning electron microscope (SEM) equipped with a cold field emission electron source. Secondary electron images were digitized and stored on a computer. Fibres were imaged either sitting on the filter membrane or after having been removed from suspension and placed on a substrate. For SEM-imaging they were coated with approximately 5–8 nm of evaporated Au or NiCr to avoid charging. The distribution of titanium fibre lengths within one batch of fibres, obtained after the cleaning and sterilization procedure called method I, was determined by measuring the length of 217 fibres from 12 random SEM images taken at 1700x magnification. The image analysis program *NIH Image* was used to measure fibre lengths from digitized electron micrographs obtained at zero tilt angle.

Fibre samples for transmission electron microscopy were prepared according to cleaning method I. Droplets (5 μl) of titanium or silicon oxide fibre suspensions in sterile water were placed onto a holey carbon film supported on a copper TEM grid and allowed to dry by evaporation in air in a Class 100 clean-room. A JEOL JEM-2000 FX transmission electron microscope (TEM) and a Link Systems AN 10000 EDX energy dispersive X-ray spectrometer were used to image and analyse the chemical composition, respectively, of the fibres. All analyses was performed using 200 keV electrons. The EDX system was operated using a beryllium window and was not able to detect oxygen, but only elements with atomic number $\geqslant 11$. The resulting composition of two titanium and two silicon oxide fibres was determined, along with contributions arising from the supporting carbon film + Cu TEM grid. Electron diffraction patterns were also recorded to characterize the crystalline status of these evaporated fibres.

Surface chemical analysis

Chemical analysis of the surface (typically an average over the top 1–3 nm, depending on the Auger electron energy) of fibres prepared by both cleaning methods was performed by scanning Auger electron spectroscopy (AES) using a PHI 660 SAM system (Physical Electronics, Eden Prairie, MN, USA). Titanium-coated silicon wafers were used as substrates for silicon oxide fibres during AES analysis. Titanium fibres were placed on either a silicon wafer or on a pure iron foil substrate. Typically a 10–20 μl droplet of fibre suspension was placed on cleaned substrates and allowed to dry by evaporation in a Class 100 clean-room. Three different types of areas were analysed on each sample: (i) fibre(s); (ii) substrate within the dried water droplet; and (iii) clean substrate outside of the droplet. The latter two were made to control for possible interference from the substrate and/or from the

dried droplets in the fibres analysis areas. Analysis was performed on a few (two to four) spots within each area and the results averaged.

The PHI 600 scanning Auger microprobe can analyse areas as small as 0.1 μm in diameter and is therefore capable of analysing individual fibres. In order to obtain a small electron beam size (preferably < 0.5 μm, the width of a fibre), analysis was performed using a primary electron beam energy of 10.0 keV and a current of 10 nA, which should give spot sizes of 0.24 μm under perfect beam alignment, filament condition, etc. However, the focused electron beam sizes obtained during this work ranged from $\leqslant 0.5$ μm to ≈ 1.75 μm. The resulting current densities are quite high and were estimated to be in the range 500–5000 mA/cm^2. Such current densities are likely to partially reduce titanium and silicon oxides due to electron-induced desorption of oxygen. Lower electron beam currents and 3 keV accelerating voltage were used for high resolution analysis of the titanium and silicon Auger peaks. The resolution of the cylindrical mirror analyser was either 0.6% for survey spectra (30–1700 eV), or 0.1% during high resolution analysis. Relative concentrations of the detected elements (0.1–1 at % detection limit, depending on element) were calculated from peak-to-peak heights in

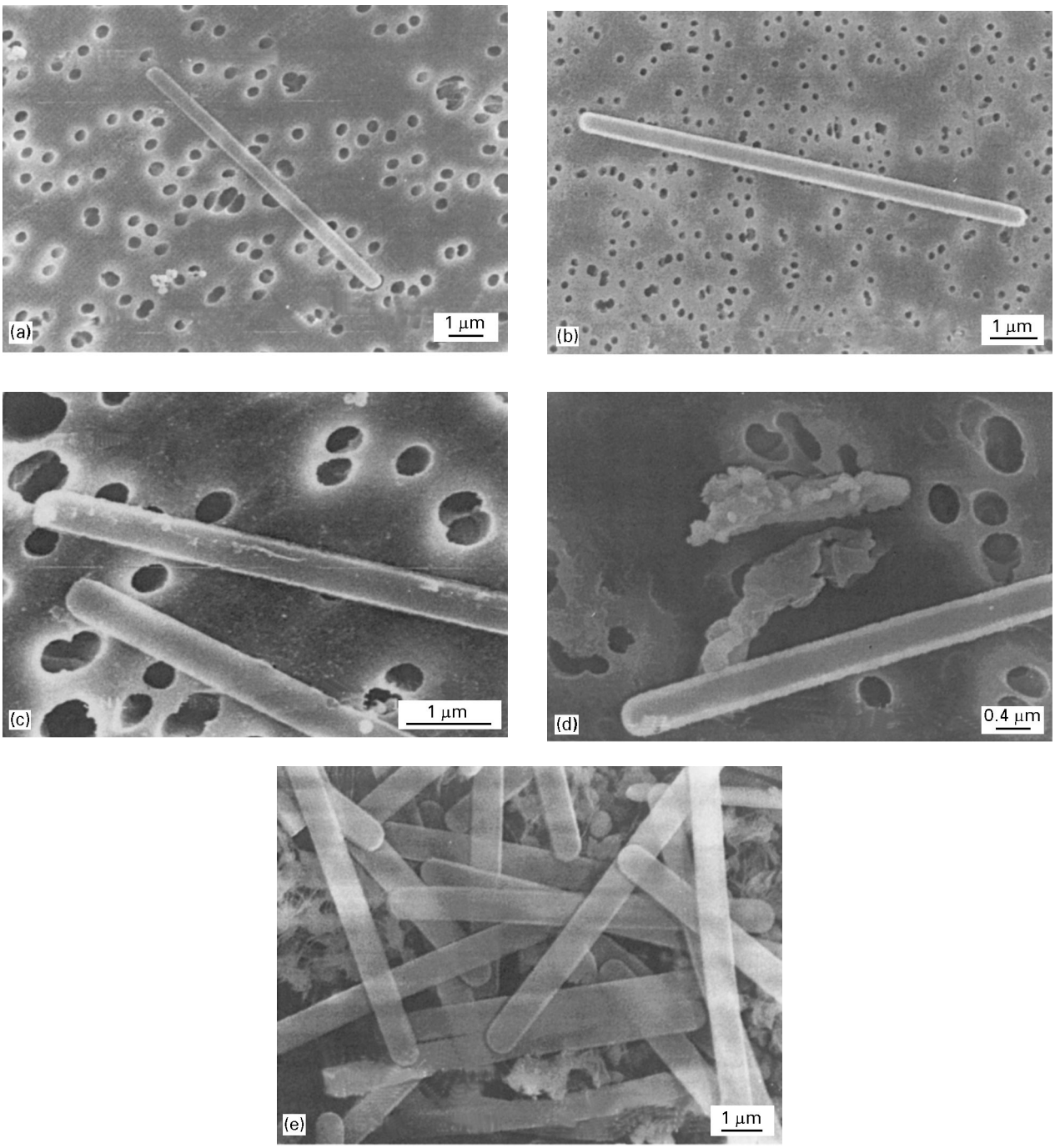

Figure 2 Scanning electron micrographs of fibres cleaned according to method I (organic solvents): (a) silicon oxide fibre sitting on a 0.4 μm pore size Isopore™ filter and (b) a titanium fibre on a 0.2 μm Isopore™ filter. Higher magnification scanning electron micrographs of fibres cleaned according to method I (organic solvents): (c) silicon oxide fibre sitting on a 0.4 μm pore size Isopore™ filter and (d) titanium fibres on a 0.4 μm Isopore™ filter. (e) Scanning electron micrograph of silicon oxide fibres cleaned according to method II (hydroxide solution) placed on a 0.5 μm Flouropore® filter.

differentiated survey spectra and tabulated elemental sensitivity factors [18]. For the case of elements such as Si and Al, low energy Auger peaks were used for quantitative analysis. Both oxide and pure elemental contributions were taken into account where appropriate. Because the diameter of the analysis area was usually larger than the width of the fibre, average compositions of the three different types of analysis areas (see above) were compared in order to isolate elemental contributions from the fibres versus those originating from the liquid in which they had been suspended, or from the underlying substrate.

The oxide thickness on titanium fibres was estimated from AES depth profile analysis performed on fibres placed onto a gold-coated silicon wafer. Sputtering and AES spectra collection were alternated as the depth profile analysis was performed through the entire thickness of the fibre (≈ 100 nm). Such spectra were collected using 3.0 keV electrons and a beam current of 94 nA. Sputtering was accomplished using a 3 keV Ar ion beam with an ion current of 0.8 μA which was rastered over the sample in an area of 2 mm × 2 mm. The sputtering rate for a Ta_2O_5 film of known thickness at the same ion gun conditions was estimated to be approximately 5.4 nm/min. A correction factor of 0.7 (based on laboratory data tabulated on reference samples comparing the sputter rates for TiO_2 and Ta_2O_5) has been applied in order to translate the Ta_2O_5 ion etch rate to titanium oxides, thus yielding an estimated etch rate of 3.8 nm/min. Oxide thickness was defined as the depth at which the oxygen signal had decreased to half its intensity detected at the surface.

3. Results

3.1. Comparison of cleaning methods I and II

The lift-off and cleaning procedure using the alkaline solution in method II is, in general, preferred over the acetone solution of method I. The removal of fibres from the bottom resist layer occurs more readily when using the alkaline resist developer. As a result, less ultrasonication is required to remove the fibres from the surface, thus reducing the risks of fibre damage. However, the Teflon™ filter membranes, required for use with such a basic solution, has so far proven to be less than optimal when it comes to placing fibres into the final suspension in sterile water (or cell culture media). This is because the Flouropore® membranes tend to fold up on themselves during the centrifugation step in water, and thus make it more difficult to remove the fibres from the membrane.

The membrane folding problem is not encountered when using the Isopore™ track-etched polycarbonate membranes in cleaning method I. However, this method requires the use of solvents as well as several solvent cleaning steps, thus increasing the total time for fibre preparation.

3.2. Fibre morphology

Silicon oxide and titanium fibres prepared by both cleaning methods are shown in Fig. 2a–e. The fibres' ends are rounded and fibres are not always planar, but tend to arc slightly, most likely due to internal stresses in the evaporated films. The top edges of the fibres appear rough or serrated, but this was only observed on fibres cleaned according to method I (Fig. 2a–d). Fibres processed by method II appeared quite smooth and without rough edges, as seen in Fig. 2e. Although the majority of fibres cleaned in organic solvents according to method I appear to be cleaned of resist (see Fig. 2a and b), some fibres do contain traces of resist (see Fig. 2c and d). Often the resist is not directly attached to the fibre, but is present on the filter. No resist debris was observed on fibres processed with hydroxide solution according to method II, but large deposits on the order of $\geqslant 40$ μm of conglomerated resist-like material were observed on the filter membrane on a few occasions.

A histogram describing the length distribution, as measured from scanning electron micrographs, of 10 μm titanium fibres cleaned by method I are shown in Fig. 3. The majority of fibres measured were 10 μm or slightly less in length. (This minute deviation in length from the nominal one is most likely only apparent due to the fact that the fibres have a curvature. Because we are measuring fibre lengths from a two-dimensional projection of curled fibres, we cannot accurately measure their true "extended" lengths.) A few fibre fragments of lengths 1.79 to 6.75 μm were also observed, and are most likely the result of occasional fibre breakage during processing and handling. Fibre widths measured from scanning electron micrographs are uniform within a given batch of fibres, but measurements between batches have shown ranges from 0.43 μm to 0.61 μm for Ti fibres, and from 0.45 up to 0.88 μm for silicon oxide fibres. This may be due to slight variations in electron beam exposure conditions, as well as slight variations during thin film deposition, between batches.

Fibres cleaned according to method I were imaged by transmission electron microscopy, the results of which are shown in Figs 4–6. The titanium fibers in

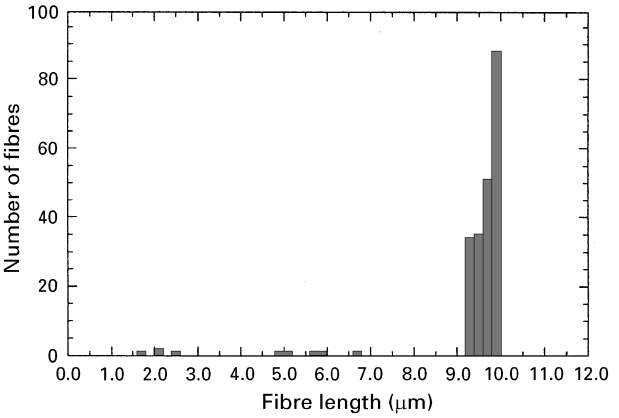

Figure 3 Distribution of fibre lengths within one batch of 10 μm long, titanium fibres after having been cleaned by method I. Fibre lengths of 217 fibres were measured using the NIH image image analysis program from 12 randomly selected, digitized scanning electron micrographs taken at 1700× magnification. Minimum 1.79; maximum 10.00; points 217; mean 9.47; median 9.74; RMS 9.55; Std deviation 1.21.

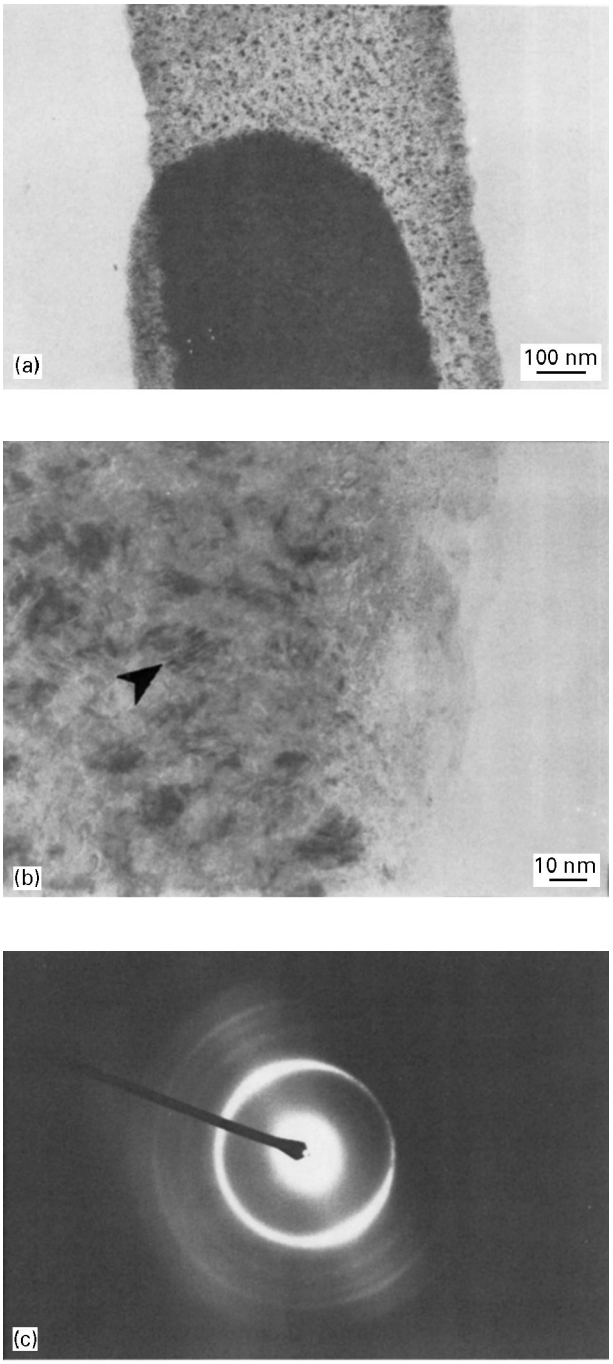

Figure 4 TEM micrographs and electron diffraction pattern of titanium fibres at (a) 68 000 × and (b) 500 000 × magnification. The arrow head in (b) indicates Moire fringes. (c) Electron diffraction pattern of titanium fibres. Refer to text for further details.

the batch analysed by TEM were measured to be 0.629–0.677 μm wide, 10.1–10.8 μm long, and 0.081–0.087 μm thick, depending on micrograph magnification. Silicon oxide fibres measured from corresponding transmission electron micrographs were 0.707–0.769 μm wide and 10.5 μm long, also depending on magnification. No silicon oxide fibres were oriented in such a way that it was possible to measure fibre thickness. The occurrence of roughened edges on only one side of the fibres is quite apparent in the titanium fibres in Fig. 4a and Fig. 5. This roughened edge is most likely a result from the first lift-off procedure (refer to Fig. 1, steps 4 to 5), and will be discussed in more detail below.

Evaporated titanium fibres appear to consist of small crystallites on the order of 10 nm in size (refer to Fig. 4a and b), most likely located within a more amorphous or microcrystalline matrix. Moire fringes originating from overlapping crystallites can be seen in Fig. 4b and are marked by an arrowhead. An amorphous-like region, varying between 10 and 30 nm thick, can be seen at the surface/edge of the titanium fibres, as clearly seen in Fig. 4b.

The diffraction pattern of a titanium fibre shown in Fig. 4c was indexed by comparing with existing powder diffraction data for metallic titanium and low oxygen-containing titanium compounds, such as Ti_2O and TiO [19]. (The diffraction pattern of Fig. 4c was obtained via a double exposure of the photographic plate. The splitting of the most intense ring $\{002\}$ is assumed to arise from the double exposure.) The diffraction pattern obtained from titanium fibres most closely resembles that of normal, hexagonal close packed (h.c.p.) α-titanium. The assignment of observed diffraction rings is shown in Table I, where the observed lines are placed next to the most likely corresponding reference lines for h.c.p. α-titanium. Since the error in d-spacing measurements was estimated to be $+/-$ 0.01 nm, the assignment of planer spacings is not entirely straightforward, especially for reflections from planes having smaller d-spacings. The titanium fibre diffraction pattern also compares fairly well with the data for Ti_2O (which corresponds to the maximum solubility of oxygen in Ti), although the match with Ti is better.

Diffraction patterns from titanium fibres (Fig. 4c) show some spotted ring formation, which at times was observed to form arched ring patterns, indicative of a polycrystalline structure having a slight preference in crystallographic orientation. Evidence for a preferred crystal growth direction can be seen in the fibre lying on its side in Fig. 5b. The crystallites appear elongated and parallel to the direction of film thickness (i.e. direction of film deposition), but when imaged from above they appear round in shape (Fig. 4a and b). Not all diffraction lines expected for α-titanium were observed. For example, reflections from the $\{010\}$ and $\{011\}$ planes were not observed. This is typical for crystalline structures containing preferred orientations. However, it is not surprising if d-spacings in the film differ somewhat compared to bulk α-titanium, due to (i) internal strain and (ii) dissolved oxygen.

No crystalline structure is detectable by electron microscopy in the silicon oxide fibres, as can be seen by the lack of contrast in Fig. 6a. The "diffraction" pattern for silicon oxide fibres shown in Fig. 6c contains diffuse rings verifying the existence of an amorphous/microcrystalline structure. (This pattern was obtained from a fibre that was positioned over a hole in the holey carbon film and therefore contains no contribution from the underlying carbon film.) As was observed on titanium fibres, there is also a surface layer of low electron density approximately 10–20 nm thick around the edge of silicon oxide fibres. This layer is clearly seen in Fig. 6b. It is not obvious, given the preparation procedure of these fibres, whether these

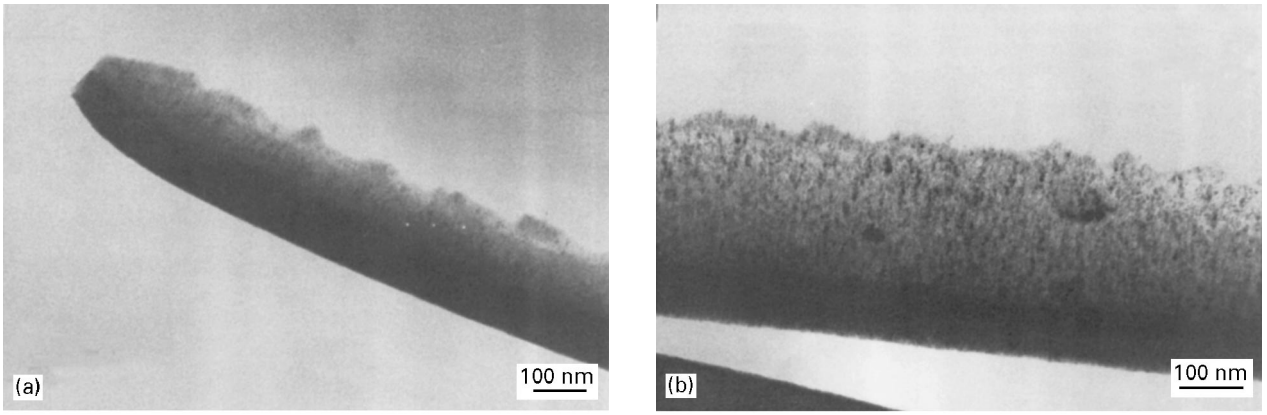

Figure 5 TEM micrographs of titanium fibres oriented at an angle to the electron beam. Images obtained at (a) 68 000 × and (b)85 000 × magnification. A raised and roughened edge can be seen on the top surface of the fibre. The crystallites appear to be elongated in the direction parallel to the thickness of the fibre, indicating a possible preferential orientation of the crystallites during growth.

TABLE I Indexed electron diffraction pattern of evaporated titanium fibre and reference h.c.p. titanium (JCPDS file #5-682) [19]

d_{hkl} (Ti fibre) (nm)	Intensity[a] (Ti fibre)	d_{hkl} (h.c.p. Ti) (nm)	Intensity[b] (h.c.p. Ti)	hkl
		0.2557	30	010
0.238	vs	0.2342	20	002
		0.2244	100	011
0.170	m	0.1726	19	012
0.146	m	0.1475	17	110
0.138	s	0.1332	16	103
0.127	vvw	0.1276	2	200
		0.1247	16	112
		0.1233	13	201
0.117	m	0.11708	2	004
		0.11220	2	202
		0.10653	3	014
		0.09895	6	203
0.096	vw	0.09458	11	211
		0.09175	10	114
		0.08927	4	212

[a]Relative intensity described as vs = very strong, s = strong, m = medium, vw = very weak, vvw = very, very weak
[b]Relative intensity described in terms of per cent, where 100 indicates greatest intensity

layers are oxygen-enriched surface regions or thin films of polymer resist which might have coated the fibres. However, the presence of a surface oxide layer on these air-exposed evaporated films is expected.

As final notes, silicon oxide fibres were observed to deform with prolonged exposure to the electron beam, especially at high magnifications. This was assumed to be the result of electron-stimulated desorption of oxygen and subsequent disintegration of the film. The small spherical particles in Fig. 6a are most likely solid polymer resist that was included in the fibre suspension.

3.3. Chemical composition of fibres

EDX-analysis

Energy dispersive X-ray spectroscopy results of the estimated bulk composition of fibres cleaned according to method I are summarized in Table II. The Cu signal from the supporting TEM grid was not included in the compositional analysis of the fibres. Titanium fibres contained ≈ 99 wt % Ti, with the remainder comprised of trace elements Cl ≈ 0.3–0.5 wt %, and < 0.2 wt % each of Fe, Co, Zn, Si, and Ni. (Note, however, that oxygen was not detected by EDX.) Detection limits for the heavier elements such as Fe, Co, Ni, Cu, and Zn are estimated on our EDX system to be ≈ 0.3 wt %, while the limit for the lighter elements is ≈ 1.0 wt %. This indicates that the trace elements detected in the fibres are below their estimated detectability limits and cannot be assumed to be significant. All trace elements except Ni were also detected in areas without fibres, where Si, Cl and Fe were the main constituents. This indicates that these elements are most likely present in the liquid in which the fibres were suspended and/or originate from the supporting carbon film and Cu TEM grid. Trace elements detected in silicon oxide fibres were Cl, Fe, Co, Ti and P, and comprised a total of 0.5 wt %. All were at levels < 0.2 wt % and thus below detection limits. As for the Ti fibres, it is believed that the trace elements of Cl, Fe, and Co originate from the liquid and/or TEM grid + carbon supporting film.

AES-analysis

Results from surface chemical analysis by AES of titanium fibres and the underlying substrate surfaces are shown in Fig. 7, and for silicon oxide fibres and substrates in Fig. 8. It is important to keep in mind that fibre analysis areas also included contributions from the underlying substrate which had been coated by the liquid droplet. It is highly likely that certain elements detected in fibre areas actually originate from the substrate and/or liquid. It is therefore necessary to compare surface compositions obtained from substrate areas without fibres, as well as substrate areas which were not covered by the drop, with the composition of fibre areas.

Substrate signals were detected in all fibre areas, as anticipated, since the electron beam size was larger than the width of the fibre. Keeping this in mind, fibre areas contained mainly 45–65% carbon, 20–30% oxygen, and 6–16% fibre-derived titanium or silicon on the respective surfaces. These values seem to

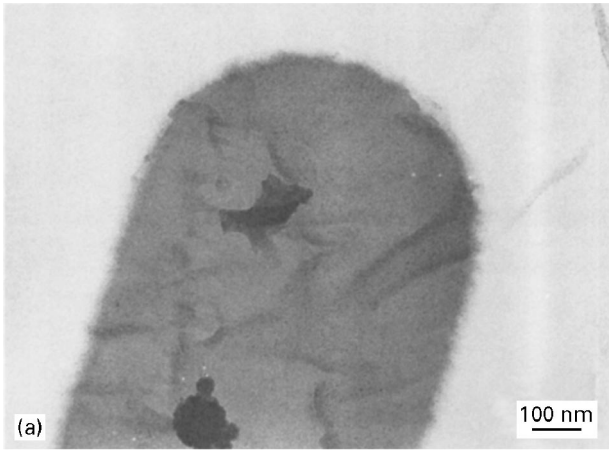

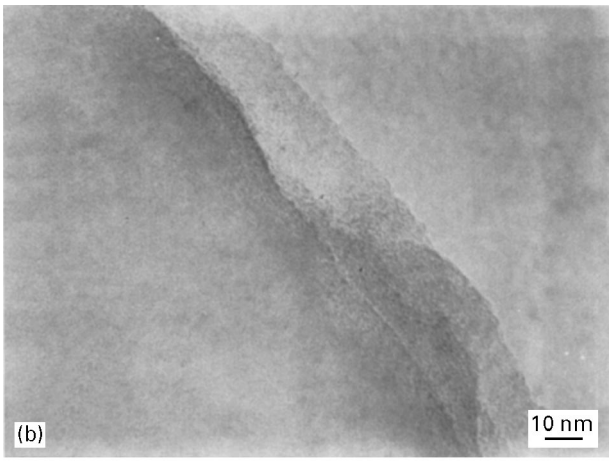

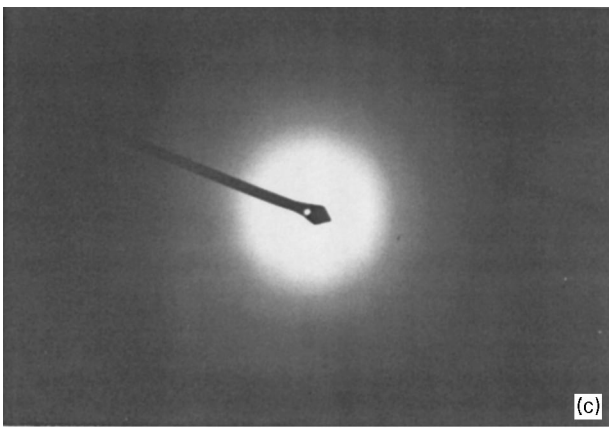

Figure 6 TEM micrographs and electron diffraction pattern of silicon oxide fibres at (a) 68 000 × and (b) 500 000 × magnification. (c) Electron diffraction pattern of silicon oxide fibres. Refer to text for details.

TABLE II EDX-determined compositional analysis of titanium and silicon oxide fibres

Element	Titanium fibre (wt %)	Carbon film + Cu grid (wt %)	Silicon oxide fibre (wt %)
Ti	98.99–99.32	–	0.03–0.19
Si	0.14–0.19	2.20	99.49–99.50
Cl	0.31–0.48	1.21	0.12–0.14
P	–	–	0.01–0.16
Fe	0.12–0.20	0.73	0.12–0.15
Co	0.14–0.15	0.35	0.10–0.18
Ni	0–0.12	–	
Zn	0–0.05	0.23	0–0.04
Cu	*	95.28	*

* Cu signal was not included in compositional analysis

contradict the possibility that the 10–20 nm layer observed on the surface of the fibres by TEM analysis could be resist. Trace elements such as S, Cl, Na, P, Ca, K, and F were detected at or near the detection limit, typically < 2 at %. Some of these elements were also detected in trace concentrations on the drop-coated substrate, but not on the clean substrate, thus indicating that they derive from the suspending liquid. Certain trace elements detected in the liquid and/or on fibres might derive from the polymer resist. According to manufacturer specifications, the resist is composed primarily of C, H, O, and Cl, and contains trace elements (< 0.1 ppm) of Si, Na, K, Ca, and Fe.

Certain exceptions were noted in the AES analysis, and include the presence of Al in all areas on the titanium fibre sample cleaned according to method I (refer to Fig. 7a). It is assumed that the silicon substrate used to mount the fibres for AES analysis was contaminated with Al, which was then detected in all analysis areas. Al was not detected on any other sample. Another exception was the detection of 5–10 at % boron in one analysis spot on titanium fibres cleaned by method I and by method II (see Fig. 7a and 7b, respectively). And finally Zn, which was detected at concentrations of ≈ 4 at % in one titanium fibre spot and one spot on the drop-coated substrate prepared by method II, must be assumed to arise from the liquid, though the assignment of this peak was questionable.

The use of iron substrates for AES analysis allowed the observation that silicon was actually present in the suspending liquid (i.e. sterile water) for titanium fibres. Silicon dust can be released from the cut edges of the silicon wafer which supports the fibres (refer to Fig. 1, step 4) during the ultrasonication steps in cleaning methods I and II. Silicon dust could then become trapped in the filter and subsequently be released with the fibres when they are placed into the final water suspension. Silicon was not detected, however, in the droplet areas on silicon oxide fibre samples, indicating that silicon dust release can vary from batch to batch. The handling of cut silicon wafers with tweezers during the processing and cleaning sequence can lead to chipping and deterioration of the silicon chip edges, thus providing additional source of silicon dust in the fibre suspension.

Titanium fibre areas contained significantly more carbon than was measured for the drop-coated substrate for both cleaning methods. However, this was not the case for silicon oxide fibres. This gives an indication that the cleaning methods might be more effective on silicon oxide fibres than titanium fibres, or that clear titanium fibres more easily react with or adsorb carbonaceous contamination than clean silicon oxide fibres. The latter is actually quite likely in view of the well-known efficient gettering action of Ti films.

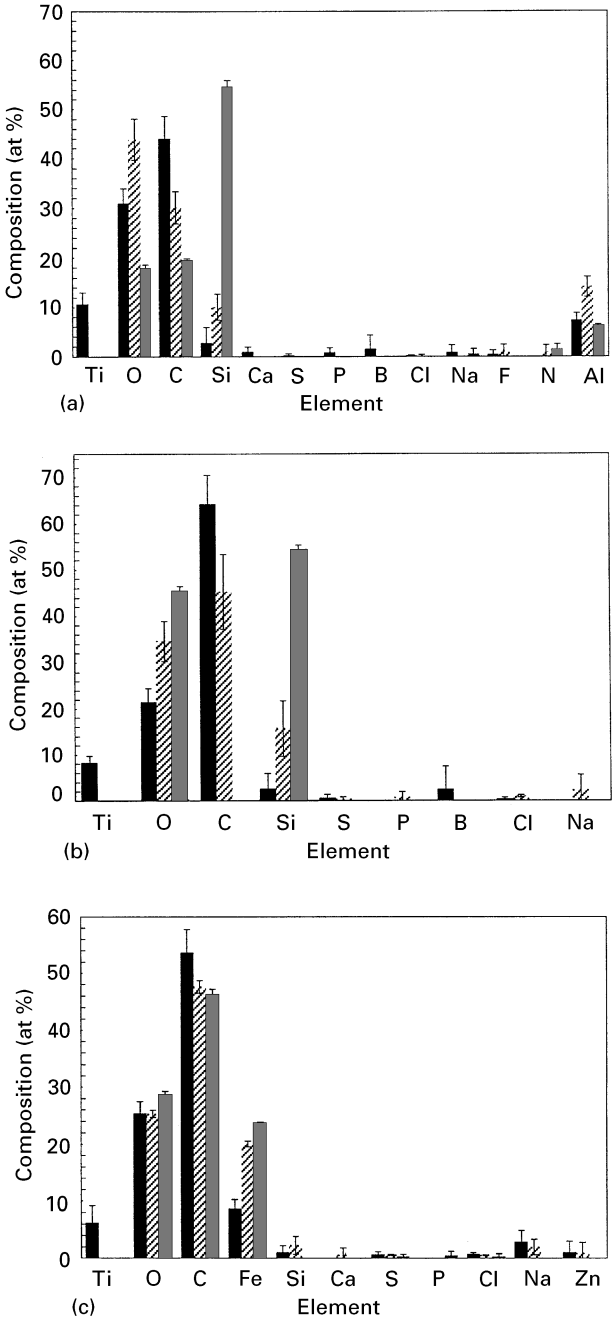

Figure 7 Surface chemical composition (at %) of titanium fibres cleaned by (a) method I or (b) method II, as determined by Auger electron spectroscopy (■). Droplets of fibre suspension were placed on a silicon wafer substrate and allowed to dry. Also included are the compositional analysis of the substrate within the dried drop (▨), and the clean substrate outside of the dried drop (▩). (c)Surface chemical composition, as determined by Auger electron spectroscopy (at %), of titanium fibres cleaned by method II but placed on an iron foil substrate in order to distinguish the Si signal from the liquid suspension (■). Also included are the compositional analysis of the substrate within the dried drop (▨), and the clean substrate outside of the dried drop (▩).

Further, chemical information can be obtained from AES spectra by analysing electron energy shifts of Auger peaks as well as peak shapes. It is quite useful for studying interactions of oxygen with solids whose Auger transitions involve valence electrons [20]. This is the case for titanium and silicon, and valence transition AES lineshapes can be used as fingerprints of the local chemical environment of the atom [20].

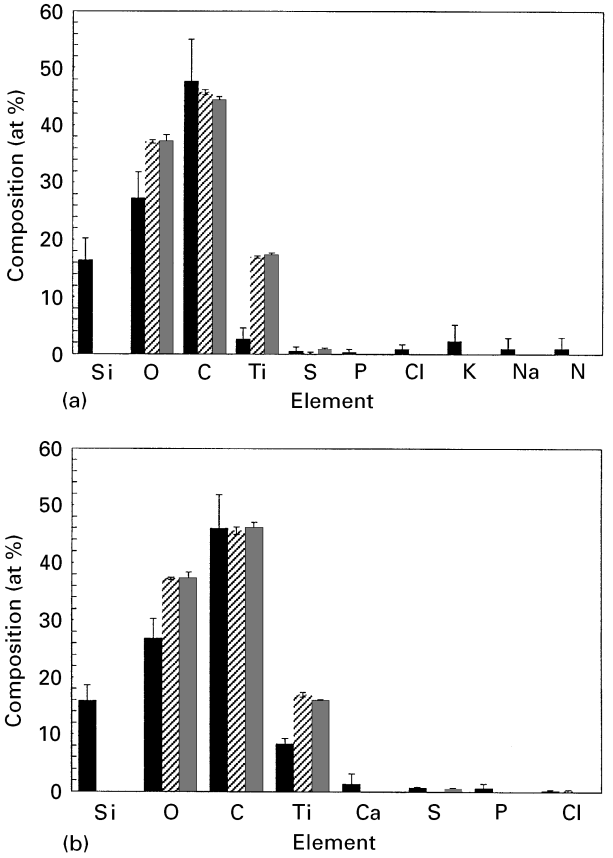

Figure 8 Surface chemical composition (at %) of silicon oxide fibres cleaned by (a) method I or (b) method II, as determined by Auger electron spectroscopy (■). Droplets of fibre suspension were placed on a titanium-coated silicon wafer substrate and allowed to dry. Also included are the compositional analysis of the substrate within the dried drop (▨), and the clean substrate outside of the dried drop (▩).

High resolution spectra of the Si LVV Auger peak obtained over different lengths of time are shown in Fig. 9. The feature located in our spectra at ≈ 82 eV is representative of a silicon oxide binding environment, while the peak at ≈ 91 eV represents elemental silicon (i.e. Si–Si bonding). The relative proportion of elemental silicon to silicon oxide peaks increases with increasing exposure time to the electron beam (as shown in Fig. 9) and with increasing current densities (results not shown). This demonstrates that silicon oxide, originally present at the fibre surface, is progressively reduced to elemental silicon during AES analysis by electron induced decomposition.

An example of the high resolution titanium spectrum obtained from titanium fibres is shown in Fig. 10. The relative heights of the LMV and LMM peaks can be used as a means to characterize the bonding environment of titanium, as the LMV transition involves valence band electrons while the LMM transition occurs between core electrons only. The relative peak-to-peak height ratio, I_{LMV}/I_{LMM}, is ≈ 1.4 for metallic titanium and ≈ 0.5 for TiO_2 [21]. The ratio of the two titanium Auger peaks for titanium fibres analysed in this work was found to vary from 0.63 to 0.99 depending on parameters of the electron beam, and increased with increasing current density and electron beam exposure time. No differences in high resolution Auger peaks were observed for fibres cleaned by method I and method II.

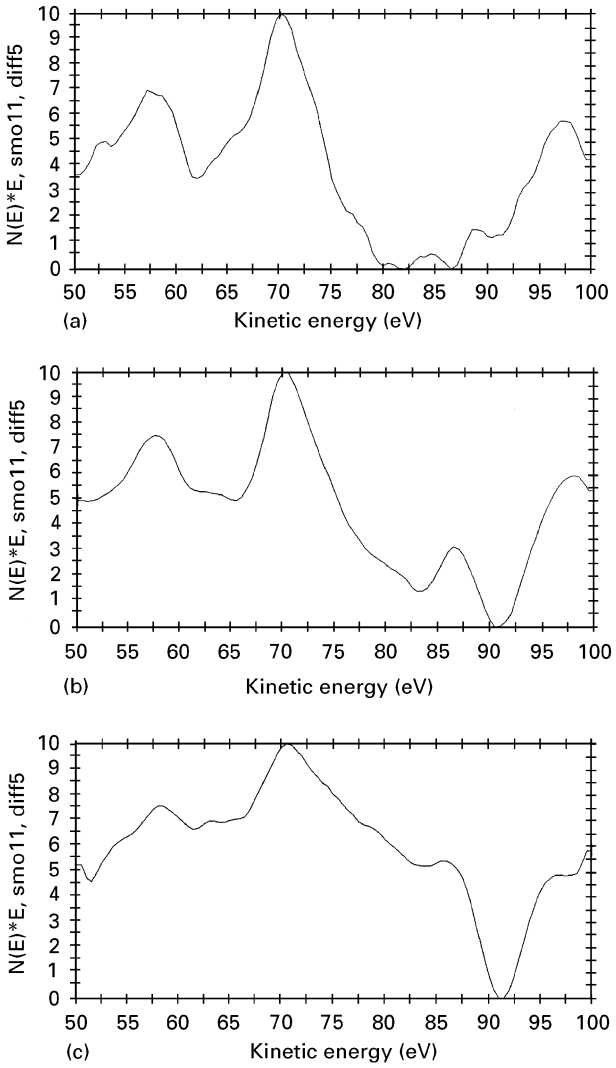

Figure 9 High resolution Auger electron spectra of the silicon LVV transition in silicon oxide fibres cleaned according to method I. Peak shape changes are attributed to changes in the chemical environment of silicon with increasing exposure time to the primary electron beam (E = 3.0 keV, I = 108 nA): (a) 40 s, (b) 200 s (c) 400 s. The gradual growth of the feature at ≈ 91 eV and subsequent decrease in the feature at ≈ 82 eV represent the change from primarily Si–O bonding to increasing concentrations of Si–Si bonds.

The Ti LMV peak consists of a double structure with peak minima at ≈ 411 eV and ≈ 417 eV, as can be seen in Fig. 10. The relative height of these peaks can also be used as a fingerprint of the oxidation state of titanium oxide surfaces [22, 23]. This double peak shape is not observed on clean, stoichiometric TiO_2. The height of the higher energy peak of the doublet, measured at ≈ 417 eV in the present work, increases with increasing current density as the TiO_2 surface is reduced by the electron beam to lower oxidation states. All high resolution spectra obtained on titanium fibres contained a double TiLMV peak shape. The relative height of the peak at ≈ 417 eV was found to increase with increasing electron current density and exposure time (results not shown). It is deduced from analysis of the high resolution titanium Auger spectrum that the surfaces of titanium fibres are covered by titanium oxide. However, it is not possible to determine the stoichiometry of the oxide from AES analysis, as we are most likely reducing the oxide under all analysis conditions.

AES depth profiling through titanium fibres show a high oxygen content throughout the thickness of the film, as can be seen in the depth profile of Fig. 11. Although the AES analysis area was wider than the fibre and also included the underlying substrate (as evidenced by the Si signal in the depth profile; the Au signal was not included for clarity), it is assumed that the oxygen signal originates from the titanium fibre and not the Au film or Ar plasma-cleaned, single-crystal Si substrate. (Adsorbed oxygen is also expected in the top monolayer of both fibre and substrate areas due to exposure to air.) Based on this assumption, a rough estimate of the relative concentrations of oxygen and titanium in the middle of the fibre was O/Ti ≈ 0.5. This ratio is indicative of Ti_2O and thus an oxygen saturated titanium metal film.

The total thickness of the fibre, estimated by the titanium signal in the depth profile and assuming an estimated sputter etch rate for titanium oxide of 3.78 nm/min, is on the order of 100 nm and is in

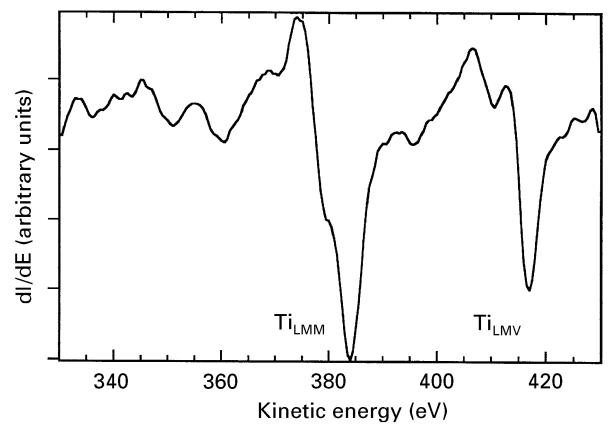

Figure 10 High resolution AES spectrum from a titanium fibre cleaned according to method I. The ratio of the intensities of the LMV and LMM peaks, as well as the shape of the LMV peak, can be used to interpret the chemical environment of titanium. The extra peak maximum at ≈ 413 eV is not present in clean titanium dioxide spectra but grows as the oxide is reduced. Refer to text for further details.

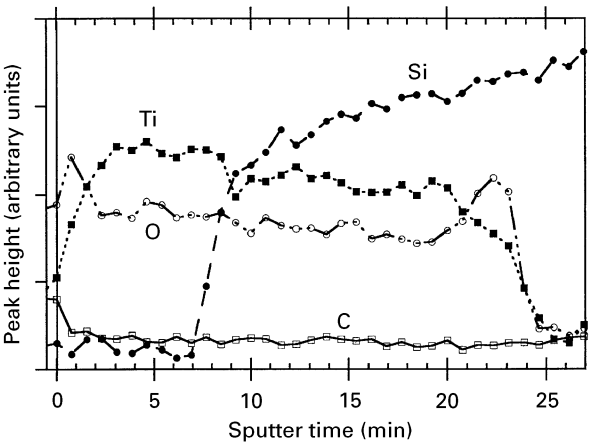

Figure 11 AES depth profile through the entire thickness of a titanium fibre showing the relative intensities (peak-to-peak heights) of the oxygen, carbon and titanium LMV Auger peaks. A high oxygen content is noted throughout the film thickness and corresponds to approximately 33 at %. Oxygen-enriched regions are present at both surfaces within the outer 10–20 nm.

agreement with the deposited amount. Distinct oxygen-rich surface layers of approximately 10–20 nm thick are present on the top and bottom surfaces of the fibre and are indicative of a surface oxide. The carbon signal has also been included in the depth profile of Fig. 11, and is elevated in intensity at the outer surface of the fibre only. This surface carbon layer is attributed to the adsorption of hydrocarbons and other carbon-containing molecules which occurs upon exposure to air, and/or in the vacuum system after film deposition.

4. Discussion

4.1. Comparison of cleaning methods

When comparing the two fibre removal and cleaning methods used in this work, it is important to note that acetone is only a weak solvent for the bottom resist on which the fibres are prepared. As a result, resist which is removed during the ultrasonication and centrifugation steps in cleaning method I might not be completely dissolved and/or filtered away by the organic solvent treatments. Such resist has been observed either attached to fibres or present on the filter membrane. The poor removal of small resist particulates could be due to the properties of the Isopore™ filter membrane. The track-etched membranes have cylindrical-shaped channels which pass directly through the filter, as compared to the more traditional filter membranes that have a much larger interconnecting pore network. Such a pore network would allow an easier passage of resist into, but perhaps not through, the membrane. In principle, any resist which is trapped on or in the filter membrane could be released during the last ultrsonication step, which is used to remove the fibres from the filter. In this way undesirable solid resist particles or other debris can arise in the final fibre suspension in sterile water.

In comparison, SAL101, the developer for the bottom resist layer, is a highly effective solvent and preferentially dissolves irradiated resist regions. Because the time which the resist and fibres are exposed to SAL101 during the fibre lift-off and cleaning procedures is considerably longer than most development times normally used for this resist, it was necessary to dilute the SAL101 to prevent the complete dissolution of the bottom resist layer. Since resist located under the fibre is also weakly irradiated during exposure of the top resist layer (refer back to Fig. 1, step 1), the use of a developer solution preferentially removes such irradiated resist lying under the fibre. This is enough to lift the fibre off of the resist layer, and at the same time prevents large quantities of dissolved resist from coming up into solution with the fibres. Except for the observation of a few very large polymer deposits, most of the resist which comes up with the fibres appears to be dissolved by the SAL101 solution and passes through, or into, the filter membrane. However, it must be pointed out that the morphology of the Isopore™ versus Fluourpore® filter membranes makes it easier to detect solid resist debris on the former.

Although lift-off and cleaning in the hydroxide solution is preferred over organic solvents in terms of reducing solid resist debris in the final fibre suspension, it is suspected that the high pH solution might also be dissolving or etching the silicon oxide and titanum fibres. The extremely smooth fibres cleaned in hydroxide solution shown in Fig. 2e give evidence to this. In principle this etching by the hydroxide can be used to our advantage to obtain more consistent fibre morphologies. However, if we clean for too long a time period in an effort to remove all traces of resist in the final fibre suspension, we run the risk of significantly altering the fibre morphology. The optimum balance of these actions needs to be studied further.

4.2. Microfabricated fibre morphology

Electron microscopy analysis of fibres reveal that the fibre corners are rounded and not square, as specified in the original CAD-drawn fibre pattern. This is a common problem in electron beam lithography and arises from what is known as proximity effects. Areas at the corners of a pattern do not receive as high an electron dose from scattered electrons as regions in the interior of the pattern, due to the lack of exposed neighbouring areas. It is often necessary to define a higher exposure dose at the corners in order to fill out the feature to its desired shape. In the present case, this can be done by adding extra features, such as rectangles or squares at the ends of the fibre to obtain square corners. Although this was successfully accomplished, it slowed down the exposure, due to an increase in the amount of data which needed to be transferred per exposure, as well as an increased exposure time due to the added areas. In order to expose sufficient fibre quantities for biological testing, the entire electron beam lithography process has had to be optimized for high speed. As a result, we decided to accept the rounded edges.

As mentioned above, fibres tend to be curved, most likely originating from internal stresses in the evaporated films. In general, large stresses are created in deposited films of any material. These originate from two sources. First, differences in thermal expansion coefficients of the deposited thin film and the substrate create stresses at the interface unless the deposition temperature and subsequent processing temperatures are the same. Second, a much larger stress may occur at the interface due to lattice mismatch between the thin film and substrate. This stress will vary across the thickness of the deposited film. Film stresses can be greater than the yield stress of the film material in bulk form, and can destroy thin films by cracking (tensile stresses) or buckling (compressive stresses). It is not surprising that the fibres produced from evaporated films in this work are slightly curved, most likely to accommodate such internal stresses which vary across the thickness of the film. The curvature of the fibres causes some minor errors in measuring fibre lengths from electron micrographs, as described in Section 3.

Difficulties in measuring exact dimensions from electron micrographs in general are related to the difficulty of obtaining proper scale calibration for each microscope at all magnifications. Digitized images transferred via an image grabber program can also distort relative X and Y scales if an improper ratio of

pixel elements in each direction is defined during image transfer. Although small differences in fibre dimensions are measured on different miroscopes and at different magnifications, the fibres generally have the intended dimensions of 10 μm in length (except for the small percentage of broken fibres due to processing and handling) and 0.1 μm thick (as verified by profilometry measurements, data not shown). However, variations in fibre widths have been observed as mentioned in Section 3. Fibre widths are uniform within a given batch of fibres, but can vary between batches due to, for example, differences in resist development time. This assumes the same electron beam exposure conditions from batch to batch, which is quite easily obtainable. However, silicon oxide fibres are often slightly wider than titanium fibres. Evaporation of oxides such as silicon oxide results in the deposition of warm or hot material that can spread when arriving on the patterned resist surface. It is more difficult to control the evaporation of a silicon oxide source material compared to metallic titanium when using electron beam evaporation methods. The beam must be rastered over a larger area in order to minimize decomposition of the source material. The assumption of a point source during evaporation of silicon oxide is therefore less valid than for titanium, and this can account for the widening of the silicon oxide features deposited through patterned resist layers. We believe both these reasons lie behind the broadening of silicon oxide fibres, as the slot width in the patterned resist layers have been equivalent for depositions of both materials. If desired, it is possible to correct for fibre widening by appropriate reduction of the width of the resist pattern used for silicon oxide depositions.

The fibres often appear with one face containing roughened or raised ridges. Roughened and raised edges of fibres are an indication of non-optimal lift-off techniques. This can result from evaporation of the fibre material at a less than optimal angle of incidence, where the deposited film might actually coat the walls of the patterned resist on one side, for example. If the raised edges occur on both edges of the top side of the fibre, this is most likely an indication of a poor resist profile, perhaps due to slight under-development of the resist pattern. Such roughened and raised edges were not observed on fibres cleaned by method II. As mentioned above, it is likely that fibres are etched slightly by this highly basic hydroxide solution, and as a result the edges are removed.

Columnar growth of deposited titanium films, i.e. individual crystal growth normal to the film surface, is typically observed for films deposited at ambient temperature [24]. If the grain structure is not perfectly random, not all reflections will appear in a diffraction pattern. Evidence for a preferred orientation of crystalline growth in the evaporated titanium films prepared in this work includes the slight arcing of diffraction rings, missing reflections in the diffraction pattern, and the appearance of parallel and elongated grains in fibres which were imaged at an angle with regard to the fibre surface. The width and spottiness of a ring pattern depend on the size and number of crystallites contributing to the diffraction image. The finer the grain size, the broader the diffraction rings, with amorphous materials giving no diffraction ring structure but rather a diffuse intensity ring. Diffraction patterns from silicon oxide fibres show no diffraction ring structure and are interpreted as being amorphous. We have not yet attempted to crystallize silicon oxide fibres, but have attempted, without success, to crystallize the same films deposited on silicon wafers (unpublished results). It is well documented that crystalline silica is more toxic than amorphous silica dusts in inhalation toxicology studies [25–27].

4.3. Chemical composition of microfabricated fibres

The evaporated titanium and silicon oxide films are quite pure in their bulk, with EDX-determined concentrations of ≈ 99 wt % Ti and ≈ 99.5 wt % Si, respectively. It should be mentioned again that oxygen is not included in this compositional analysis. Minor levels of impurities were detected ($< 0.5\%$ each in titanium fibres and $< 0.2\%$ each in silicon oxide fibres), most of which were at or below the detection limit of EDX, and were also detected in the underlying substrate, and could therefore be attributed to the substrate and not to the fibre. The oxygen content remains quite high through the thickness of the fibre, and this is quite common for evaporated or sputtered films of reactive materials such as titanium [28]. While electron diffraction patterns showed no indication of the presence of TiO_2 phases and were best matched to patterns from metallic titanium, they also showed some similarities with the diffraction pattern for Ti_2O, i.e. an oxygen-saturated h.c.p. titanium lattice.

Surface chemical analysis by Auger electron spectroscopy shows that the surface of the fibres contain mainly carbon and oxygen in addition to titanium or silicon, depending on fibre material. Compared to silicon oxide fibres, titanium fibre areas had significantly higher surface carbon levels than the surrounding underlying substrate. The carbon-containing contamination most likely originates from a combination of remaining resist, adsorbed alcohol and/or hydrocarbon molecules from the environment. It is present as one or a few monolayers. Analysis of Auger peak shapes indicates the existence of oxides at the surface of both fibre types, but the exact nature of these oxides need to be further evaluated by, for example, X-ray photoelectron spectroscopy (XPS). However, fairly large quantities of fibres are required for XPS analysis because of its large analysis area (≈ 0.8 mm diameter) while AES analysis with the scanning Auger microprobe can be made on an individual fibre. The surface layers of ≈ 10–20 nm thick observed on titanium fibres in TEM most likely are the ≈ 10–20 nm thick oxygen-rich layers detected by AES depth profiling, i.e. a surface oxide. It is then most likely that the surface layers observed on silicon oxide fibres in TEM are also oxygen-rich layers and not resist coatings. This is supported by the absence of increased levels of carbon in fibre areas compared to drop and substrates areas in the AES analysis.

5. Summary

Although much detail was presented above on the morphological and chemical analysis of microfabricated fibres, a brief summary of the more relevant results will be given here. The 10 μm long fibres produced in titanium and silicon oxide were found to contain rounded corners, a slight curvature along the length of the fibre, and roughned edges. Fibres were practically monodisperse in length, with only a few exceptions of broken fibres. However variations in fibre width was found to exist between production lots (i.e. wafers) and was in the range $+/-$ 0.1–0.2 μm, depending on fibre material. In general, silicon oxide fibres tended to be approximately 2% wider than titanium fibres.

Titanium fibres are nanocrystalline, with crystallites on the order of 10 nm in size, while silicon oxide fibres are amorphous. Both fibres contain amorphous oxygen-rich surface layers $\approx$ 10–30 nm in thickness. Fibres are $\approx$ 99–99.5% pure in composition (not including bulk oxygen content), as determined by EDX analysis, but contain trace levels of impurities at or below detection limits of the method, most likely deriving from the suspending liquid, and one to a few monolayers of carbon-containing contamination on their surfaces, the latter measured by AES. Remaining resist and silicon (dust) contamination from the processing procedure appear to be present in the final fibre suspension, although their quantities vary between fibre batches. Such contamination is clearly the result of the "reverse" filtration procedure, where substances retained on, or in, the filter are collected instead of the filtered liquid.

Cleaning fibres in hydroxide solution is preferred over organic solvents because (i) fibres are more easily removed from the substrate, (ii) resist is more efficiently removed from the fibres, (iii) the cleaning process is easier with just two solutions, (iv) the solution is more environment friendly, and (v) edge features are removed from the tops of the fibres. However, the hydroxide solution appears to etch the fibres and requires the use of chemically resistant filter membranes (i.e. Teflon™) which are hydrophobic and are more difficult to handle with aqueous solution.

The lift-off and cleaning methods developed to date have produced relatively clean fibres of uniform shapes and dimensions, and with high fibre retention rates compared to previously used methods. However, further improvements in the processing methods can be made to reduce the carbon and sporadic silicon contamination detected in the final fibre suspension. This could be achieved by a different choice of substrate material and/or form, for example, one which did not contain silicon and would not require cutting away lithographically patterned regions of the substrate.

Acknowledgements

The authors thank Tanya Kuzmina, Eva Olsson, and Björn-Owe Aronsson for their assistance with the fibre preparation, TEM/EDX analysis, and AES data analysis, respectively. This research has been funded by the Swedish Biomaterials Consortium, which is supported by NUTEK (Swedish National Board for Industrial and Technical Development) and NFR (Swedish Natural Science Research Council).

References

1. J. E. CRAIGHEAD and B. T. MOSSMAN, *New Eng. J. Med.* **306** (1982) 1446.
2. A. OHLIN, O. JOHNELL and U. H. LERNER, *Clin. Orthop. Rel. Res.* **253** (1990) 287.
3. J. A. SAVIO III, L. M. OVERCAMP and J. BLACK, *Clin. Matls.* **15** (1994) 101.
4. M. C. JAURAND, in "Non-occupational exposure to mineral fibres", edited by J. Bignon, J. Peto and R. Saracci (IRAC, Lyon, 1989) p. 54.
5. M. F. HOCHELLA, in "Mineralogical Society of America reviews in mineralogy", edited by G. D. Gutherie and B. T. Mossman (Mineralogical Society of America, Chelsea, 1993) p. 275.
6. B. KASEMO and J. LAUSMAA, *Environ. Health Perspect.* **102** (1994) 41.
7. B. FUBINI, in "Fiber toxicology" (Academic Press, New York, 1993) p. 229.
8. B. KASEMO and J. LAUSMAA, *Mater. Sci. Engng.* **C1** (1994) 115.
9. B. D. RATNER, *J. Biomed. Mater. Res.* **27** (1993) 837.
10. M. F. STANTON, M. LAYARD, A. TEGERIS, E. MILLER, M. MAY, E. MORGAN and A. SMITH, JNCI **67** (1981) 965.
11. A. R. BRODY, Personal communication.
12. W. M. MOREAU, in "Semiconductor lithography: principles, practices, and materials" (Plenum Press, New York, 1988).
13. J. GOLD, B. NILSSON and B. KASEMO, *J. Vac. Sci. Technol. A* **13** (1995) 2638.
14. V. TIMBRELL, *Ann. NY Acad. Sci.* **132** (1965) 255.
15. D. NADEAU, D. L. FOUQUETTE-COUTURE, D. PARADIS, J. KHORAMI, D. LANE and J. DUNNIGAN, *Drug Chem Toxicol.* **10** (1987) 49.
16. A. S. SHANBHAG, J. J. JACOBS, J. BLACK, J. O. GALANTE and T. T. GLANT, *J. Biomed. Mater. Res.* **28** (1994) 81.
17. J. M. G. DAVIS and M. -C. JAURAND (eds), "Cellular and molecular effects of mineral and synthetic dusts and fibres", NATO ASI Series, Vol. H 85 (Springer Verlag, Berlin, 1994).
18. L. E. DAVIS, N. C. MACDONALD, P. W. PALMBERG, G. E. RIACH and R. E. WEBER, in "Handbook of Auger electron spectroscopy" (Physical Electronics, Eden Prairie, 1978).
19. JCPDS, "Power diffraction file: inorganic materials" (JCPDS International Centre for Diffraction Data, Swarthmore, 1979).
20. H. H. MADDEN, *J. Vac. Sci. Technol.* **18** (1981) 677.
21. B. -O. ARONSSON, PhD Thesis, Chalmers University of Technology, Göteborg, 1995.
22. J. LAUSMAA, B. KASEMO and H. MATTSON, *Appl. Surf. Sci.* **44** (1990) 133.
23. C. RAO and D. SARMA, *Phys. Rev. B* **25** (1982) 2927.
24. R. BRUINSMA, R. P. U. KARUNASIRI and J. RUDNICK, in "Kinetics of ordering and growth at surfaces", edited by M. G. Lagally (Plenum Press, New York, 1990) p. 395.
25. R. C. BROWN, E. A. SARA, J. A. HOSKINS, C. E. EVANS, J. YOUNG, J. J. LASKOWSKI, R. ACHESON, S. D. FORDER and A. P. ROOD, *Ann. Occup. Hyg.* **36** (1992) 115.
26. M. D. ENGLEN, S. M. TAYLOR, W. W. LAEGREID, R. M. SILFLOW and R. W. LEID, *Exp. Lung Res.* **16** (1990) 691.
27. V. VALLYATHAN, J. F. MEGA, X. SHI and N. S. DALAL, *Amer. J. Respir. Cell Mol. Biol.* **6** (1992) 404.
28. C. P. LOFTON and W. E. SWARTZ JR, *Thin Solid Films* **52** (1978) 271.

Received 17 May
and accepted 16 July 1996